2008 American Control Conference
Westin Seattle Hotel, Seattle, Washington, USA
June 11-13, 2008

The Design and Implementation of Driving Mode Control for Vibrational Gyroscopes[1]

Lili Dong[2, *], *Member, IEEE,* Qing Zheng[2], *Student Member, IEEE*, David Avanesov[2], S*tudent Member, IEEE*

Abstract—**The paper presents a novel oscillation controller for controlling the driving mode (or drive axis) of a vibrational gyroscope to oscillate at a desired trajectory. The controller consists of a PD controller and an online Extended State Observer (ESO). The ESO is used to estimate the system states and the discrepancy between the real system and the mathematical model of the gyroscope. The PD controller drives the estimated discrepancy and the tracking error of the output of the driving mode to zero. Since the controller design does not require exact information of system parameters, it is very robust against structural uncertainties of the gyroscope. The convergence of the estimation error of the ESO and the stability of the control system are theoretically proven. The controller is validated by software and analog hardware implementations on a vibrational piezoelectric beam gyroscope.**

Keywords: Vibrational gyroscopes, oscillation controller, extended state observer, analog implementation.

I. INTRODUCTION

MEMS gyroscopes, also termed as vibrational gyroscopes, use vibrating elements to sense rotation rates. Since the gyroscopes don't have bearings, they can be easily miniaturized and batch fabricated on silicon or poly-silicon. The absence of bearing friction in MEMS gyroscopes also eliminates the principle cause of power consumption [1]. With the advantages of small size, low cost and low power consumption, the MEMS gyroscopes have found broad applications in consumer and automotive markets. Some of the well known automotive applications include vehicle stability control, navigation assist, and rollover detection. Examples of consumer applications are 3D input devices, robots, and camcorder stabilization. However, due to the high production cost and low performance and reliability [1], most of the applications of the MEMS gyroscopes have not reached any significant volume. The effects of imprecise micro-fabrication and environmental variations degrade the performance of the MEMS gyroscope and consequently cause measurement errors of rotation rates [2]. Traditional mechanical balancing could reduce the effects of a limited amount of the imperfection. But it is time consuming, expensive and difficult to perform on a small-size MEMS gyroscope [3].

[1]The work is supported by Ohio ICE (Instrumental, Control, and Electronic) consortium under grant 0260-0652-10.

[2]The authors are with the Department of Electrical and Computer Engineering at Cleveland State University, Cleveland, OH 44115.

*Corresponding author. Email: L.Dong34@csuohio.edu.

Since the early 1990s, more and more researchers have been trying to improve the performance of the vibrational gyroscopes through control electronics. In [4, 5], a typical Phase Locked Loop (PLL) is used to adjust the input frequency till the output of drive axis is -90^0 out of phase with the input indicating the resonance, and an Automatic Gain Control (AGC) loop is used to regulate the output amplitude. In this system, the input frequency is dependent on the mechanics of device and changing with environmental variations. As an alternative to the PLL control, an adaptive controller is developed in [6] to tune the closed-loop frequency of drive axis to a fixed frequency chosen by the designer. But in [6], the amplitude regulation of the drive axis is disregarded. In [7], an adaptive oscillation controller is introduced without requiring an external driving input. However, the controller assumed an ideal model of the drive axis and did not consider the mechanical coupling terms between both axes. In [8], an adaptive controller is designed to drive the vibrations of two axes of the gyroscope operating in an adaptive mode where the movements of the mass along two axes are equal. However, most reported MEMS gyroscopes are operating in a conventional mode [3] where the movement of the mass along the drive axis is relatively large and the movement along the sense axis is very small. In [9], an adaptive control system is designed for both axes of the conventional MEMS gyroscopes where the mechanical thermal noise and parameter variations are neglected.

In this paper, we aim to design an oscillation controller for the drive axis of the conventional MEMS gyroscope where the coupling terms, the noise, and the parameter variations are considered. We will apply a recently reported Active Disturbance Rejection Controller (ADRC) [10] to the drive axis. The ADRC is a combination of a linear observer and a PD controller. The disturbance represents any discrepancies between the mathematical model and a real system, hence is also taken as uncertainties of the system. The controller is built on the observed disturbance and compensates for it in real time. As reported in [11, 12], ADRC has been successfully applied to macro-systems such as motion control, aircraft flight control, and jet engine control etc because of its robustness against parameter variations and its few numbers of tuning parameters during implementation. It is the first time we modify the controller and extend its use to the MEMS gyroscopes.

This paper is organized as follows. The dynamics of MEMS gyroscope is explained in Section II. The oscillation controller is presented in Section III. Simulation results are shown in Section IV. It is followed by the analog implementation and experimental results in Section V. Finally some concluding remarks are given in Section VI.

II. THE DYNAMICS OF MEMS GYROSCOPES

A MEMS gyroscope can be understood as a silicon proof mass attached to a rigid frame through springs and dampers. The mechanical structure of a MEMS gyroscope is shown in Fig.1. The proof mass is driven into resonance along the drive axis (X axis) in order to obtain the largest response and phase synchronization. As the rigid frame rotates around rotation axis (perpendicular to the page) with the rate of Ω, a Coriolis acceleration is produced along sense axis (Y axis), which is perpendicular to both drive and rotation axes. The Coriolis acceleration provides the information of rotation rate. So we can determine the rotation rate through sensing the vibration of sense axis.

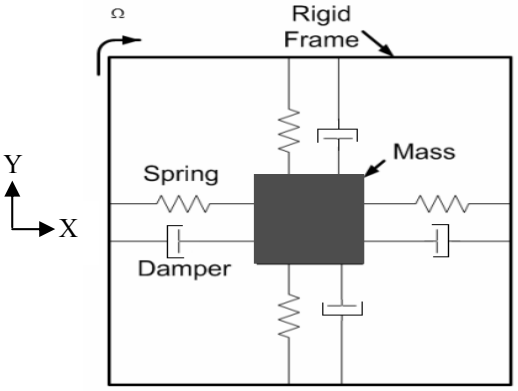

Fig. 1: Mass-spring-damper structure of vibrational MEMS gyroscopes

Assuming the natural frequencies of both axes are same and the sense axis is operating in open loop, the vibrational MEMS gyroscope is modeled as

$$\begin{aligned} \ddot{x} + 2\varsigma\omega_n\dot{x} + \omega_n^2 x + \omega_{xy} y - 2\Omega\dot{y} &= \frac{K}{m}u_d \\ \ddot{y} + 2\varsigma\omega_n\dot{y} + \omega_n^2 y + \omega_{xy} x + 2\Omega\dot{x} &= \frac{1}{m}N(t) \end{aligned} \tag{1}$$

where x and y are the displacement outputs of drive and sense axes respectively, $2\Omega\dot{x}$ and $2\Omega\dot{y}$ are Coriolis accelerations, Ω is the rotation rate, ω_n is the natural frequency of drive and sense axes, $\omega_{xy}y$ and $\omega_{xy}x$ are Quadrature errors caused by spring coupling terms between two axes, ς is damping coefficient typically ranging from 10^{-3} through 10^{-1}, m is the mass of the MEMS gyroscope, K is the controller gain including forward gain and actuator and sensor scale factors, and u_d is the control input for drive axis. The Quadrature errors are constant unknown signals, which need to be canceled out in control effort u_d. The rotation rate Ω is assumed to be a constant unknown signal. In (1), mechanical thermal noise on the sense axis is represented by the random force N(t). The drive axis displacement x(t) is usually so large that the effects of thermal noise on the drive axis are negligible and are disregarded [14]. For the conventional mode of operation, the displacement of the sense axis is very small. It tends to be contaminated by the noise. Hence the noise on the sense axis can not be ignored.

Our control objective is to force the drive axis to oscillate at specified amplitude and resonant frequency in the presences of parameter variations, mechanical couplings, and mechanical-thermal noise.

III. OSCILLATION CONTROLLER

Both drive and sense axes of MEMS gyroscopes can be taken as lightly damped second-order systems. They are governed by the Newtonian law of motion. Then we could rewrite the drive axis model as

$$\ddot{x} = f(\dot{x}, x, d) + bu_d \tag{2}$$

where b is the coefficient of the controller ($b=K/m$), d is an external disturbance [12], and $f(x, \dot{x}, d)$ (or simply denoted as f) accounts for all the other forces excluding the control effort u_d [10], which is

$$f = -2\varsigma\omega_n\dot{x} - \omega_n^2 x - \omega_{xy} y + 2\Omega\dot{y}. \tag{3}$$

We assume b is known. If an observer is designed to estimate the f, we can take u_d as

$$u_d = \frac{1}{b}(-\hat{f}(\dot{x}, x, d) + u_0), \tag{4}$$

where $\hat{f}$ is the estimated f, u_0 is a controller to be determined. Then (3) becomes

$$\ddot{x} = f(\dot{x}, x, d) - \hat{f}(\dot{x}, x, d) + u_0 \approx u_0. \tag{5}$$

We suppose a desired signal r has the resonant frequency ω and the maximum amplitude A that the drive axis could output. And r is represented by

$$r = A\sin(\omega t). \tag{6}$$

Then our control goal is to drive the output signal x to the signal r. We have tracking error $e=r-x$. We can employ a common Proportional Derivative (PD) controller for u_0 to drive tracking error e to zero. The controller is

$$u_0 = k_p e + k_d \dot{e}. \tag{7}$$

If we take the partially unknown f as a generalized disturbance or the discrepancy between the real system and its nominal model, the controller will estimate it and compensate for it actively, hence the name ADRC.

A. Extended State Observer

The effectiveness of ADRC is dependent on the accurate estimation of the f. Consequently an Extended State Observer (ESO) is developed to estimate the disturbance f in real time. This can be achieved by using the linear state space representation of drive axis model and augmenting the state variables to include f [10]. We suppose $\dot{f}$ is unknown and bounded. Let $x_1=x$, $x_2=\dot{x}$, $x_3=f$, and $X=[x_1, x_2, x_3]^T$, we have

$$\begin{aligned} \dot{X} &= AX + Bu_d + Eh \\ z &= CX \end{aligned} \tag{8}$$

where

$$A = \begin{bmatrix} 0 & 1 & 0 \\ 0 & 0 & 1 \\ 0 & 0 & 0 \end{bmatrix}, B = \begin{bmatrix} 0 \\ b \\ 0 \end{bmatrix}, C = [1 \quad 0 \quad 0], E = \begin{bmatrix} 0 \\ 0 \\ 1 \end{bmatrix}, h = \dot{f}.$$

Based on (8), a state observer is given by

$$\begin{aligned}\dot{\hat{X}} &= A\hat{X} + Bu_d + L(z-\hat{z}) \\ \hat{z} &= C\hat{X}\end{aligned} \tag{9}$$

where the estimated state vector is $\hat{X} = [\hat{x}_1, \hat{x}_2, \hat{x}_3]^T$, and the vector of observer gain is $L= [l_1, l_2, l_3]^T$. We need to notice that the key part of (9) is the third state of observer $\hat{x}_3$, which is used to approximate *f*. The characteristic polynomial of observer is represented by

$$p(s) = s^3 + \alpha_1 s^2 + \alpha_2 s + \alpha_3. \tag{10}$$

If the observer gains are selected as $l_1 = 3\omega_o$, $l_2 = 3\ \omega_o^2$, $l_3 = \omega_o^3$, and $\omega_o > 0$, the characteristic polynomial becomes

$$p(s) = (s+\omega_o)^3. \tag{11}$$

Therefore we can change the observer gains through tuning the unique parameter ω_0, which is the bandwidth of the observer.

B. Control Algorithm

After the observer is designed, the oscillation control of drive axis given by (4) becomes

$$u_d = \frac{1}{b}(-\hat{x}_3 + u_0). \tag{12}$$

In order to minimize the number of tuning parameters of the controler u_0, the controller parameters are chosen as $K_p=\omega_c^2$ and $K_d=2\omega_c$, where $\omega_c > 0$.

Then (7) becomes

$$u_0 = \omega_c^2 e + 2\omega_c \dot{e}. \tag{13}$$

Since the velocity of the movement along drive axis is not measurable, the controller u_0 built on the observed velocity is shown as

$$u_0 = \omega_c^2 (r - \hat{x}_1) + 2\omega_c (\dot{r} - \hat{x}_2) \tag{14}$$

Assuming accurate estimation of the states, the ideal closed-loop transfer function of controller is

$$G(s) = \frac{x}{r} = \frac{\omega_c^2 + 2\omega_c s}{s^2 + 2\omega_c s + \omega_c^2}. \tag{15}$$

From (15), we can see that this is a typically second-order critical-damping control system, where ω_c is the only one tuning parameter for the control input u_d. The details about how to tune the parameters of ADRC are introduced in [11].

C. Stability Analysis

1) Convergence of the ESO

Let $\tilde{x}_i t) = x_i(t) - \hat{x}_i(t)$, *i=1, 2, 3*. From (8) and (9), the observer estimation error dynamics can be shown as

$$\begin{aligned}\dot{\tilde{x}}_1 &= \tilde{x}_2 - l_1\tilde{x}_1 \\ \dot{\tilde{x}}_2 &= \tilde{x}_3 - l_2\tilde{x}_1 \\ \dot{\tilde{x}}_3 &= h - l_3\tilde{x}_1.\end{aligned} \tag{16}$$

Now let us scale the observer estimation error $\tilde{x}_i(t)$ by ω_o^{i-1}, i.e., let $\varepsilon_i(t) = \dfrac{\tilde{x}_i(t)}{\omega_0^{i-1}}, i = 1,2,3.$ Then (16) can be rewritten as

$$\dot{\varepsilon} = \omega_0 A_\varepsilon \varepsilon + B_\varepsilon \frac{h(X,d)}{\omega_0^2}, \tag{17}$$

Where $\varepsilon = \begin{bmatrix}\varepsilon_1 \\ \varepsilon_2 \\ \varepsilon_3\end{bmatrix}$, $A_\varepsilon = \begin{bmatrix}-3 & 1 & 0 \\ -3 & 0 & 1 \\ -1 & 0 & 0\end{bmatrix}$, $B_\varepsilon = \begin{bmatrix}0 \\ 0 \\ 1\end{bmatrix}$.

Theorem 1: Assuming *h(X,d)* is bounded, there exists a constant $\sigma > 0$ and a finite time $T_1 > 0$ such that $|\tilde{x}_i(t)| \le \sigma, i = 1,2,3, \forall t \ge T_1 > 0$ and $\omega_o > 0$. Furthermore, $\sigma = \mathrm{O}\left(\dfrac{1}{\omega_o^k}\right)$, for some positive integer k.

Proof: Solving (17), we can obtain

$$\varepsilon(t) = e^{\omega_o A_\varepsilon t}\varepsilon(0) + \int_0^t e^{\omega_o A_\varepsilon (t-\tau)} B_\varepsilon \frac{h\left(X(\tau), d\right)}{\omega_o^2} d\tau. \tag{18}$$

Let

$$p(t) = \int_0^t e^{\omega_o A_\varepsilon (t-\tau)} B_\varepsilon \frac{h\left(X(\tau), d\right)}{\omega_o^2} d\tau. \tag{19}$$

Since $h\left(X(\tau), d\right)$ is bounded, that is, $\left|h\left(X(\tau), d\right)\right| \le \delta$, where δ is a positive constant, we have

$$\begin{aligned}|p_i(t)| &\le \frac{\int_0^t \left[e^{\omega_o A_\varepsilon (t-\tau)} B_\varepsilon\right]_i \left|h\left(X(\tau), d\right)\right| d\tau}{\omega_o^2} \\ &\le \frac{\delta}{\omega_o^3}\left[\left|\left(A_\varepsilon^{-1} B_\varepsilon\right)_i\right| + \left|\left(A_\varepsilon^{-1} e^{\omega_o A_\varepsilon t} B_\varepsilon\right)_i\right|\right],\end{aligned} \tag{20}$$

where $i = 1,2,3$. Since $A_\varepsilon^{-1} = \begin{bmatrix}0 & 0 & -1 \\ 1 & 0 & -3 \\ 0 & 1 & -3\end{bmatrix}$, one has

$$\left|\left(A_\varepsilon^{-1} B\right)_i\right| = \left|\begin{bmatrix}-1 \\ -3 \\ -3\end{bmatrix}_i\right| = \begin{cases}1|_{i=1} \\ 3|_{i=2,3}\end{cases}. \tag{21}$$

Since matrix A_ε is Hurwitz, there exists a finite time $T_1 > 0$ such that

$$\left|\left[e^{\omega_o A_\varepsilon t}\right]_{ij}\right| \le \frac{1}{\omega_o^3} \tag{22}$$

for all $t \ge T_1$, $i, j = 1,2,3$. Hence

$$\left|\left[e^{\omega_o A_\varepsilon t} B\right]_i\right| \le \frac{1}{\omega_o^3} \tag{23}$$

for all $t \ge T_1$, $i = 1,2,3$. Note that T_1 depends on $\omega_o A_\varepsilon$.

Let $A_\varepsilon^{-1} = \begin{bmatrix}s_{11} & s_{12} & s_{13} \\ s_{21} & s_{22} & s_{23} \\ s_{31} & s_{32} & s_{33}\end{bmatrix}$ and $e^{\omega_o A_\varepsilon t} = \begin{bmatrix}d_{11} & d_{12} & d_{13} \\ d_{21} & d_{22} & d_{23} \\ d_{31} & d_{32} & d_{33}\end{bmatrix}$.

One has

$$\left|\left(A_\varepsilon^{-1}e^{\omega_o A_\varepsilon t}B_\varepsilon\right)_i\right| = \left|s_{i1}d_{13}+s_{i2}d_{23}+s_{i3}d_{33}\right| \le \begin{cases}\left|\frac{1}{\omega_o^3}\right|_{i=1}\\ \left|\frac{4}{\omega_o^3}\right|_{i=2,3}\end{cases} \tag{24}$$

for all $t \ge T_1$. From (20), (21) and (24), we obtain

$$\left|p_i(t)\right| \le \frac{\delta}{\omega_o^3}\left[3+\frac{4}{\omega_o^3}\right] = \frac{3\delta}{\omega_o^3}+\frac{4\delta}{\omega_o^6} \tag{25}$$

for all $t \ge T_1,\ i=1,2,3$.

Let $\varepsilon_{sum}(0) = \left|\varepsilon_1(0)\right|+\left|\varepsilon_2(0)\right|+\left|\varepsilon_3(0)\right|$. It follows that

$$\left|\left[e^{\omega_o A_\varepsilon t}\varepsilon(0)\right]_i\right| = \left|d_{i1}\varepsilon_1(0)+d_{i2}\varepsilon_2(0)+d_{i3}\varepsilon_3(0)\right| \le \frac{\varepsilon_{sum}(0)}{\omega_o^3} \tag{26}$$

for all $t \ge T_1,\ i=1,2,3$. From (18), one has

$$\left|\varepsilon_i(t)\right| \le \left|\left[e^{\omega_o A_\varepsilon t}\varepsilon(0)\right]_i\right| + \left|p_i(t)\right|. \tag{27}$$

Let $\tilde{X}_{sum}(0) = \left|\tilde{X}_1(0)\right|+\left|\tilde{X}_2(0)\right|+\left|\tilde{X}_3(0)\right|$. According to $\varepsilon_i(t) = \dfrac{\tilde{X}_i(t)}{\omega_o^{i-1}}$ and (25)-(27), we have

$$\begin{aligned}\left|\tilde{X}_i(t)\right| &\le \left|\frac{\varepsilon_{sum}(0)}{\omega_o^3}\right|\omega_o^{i-1}+\left|p_i(t)\right|\omega_o^{i-1}\\ &\le \left|\frac{\tilde{X}_{sum}(0)}{\omega_o^3}\right|+\frac{3\delta}{\omega_o^{4-i}}+\frac{4\delta}{\omega_o^{7-i}}\\ &= \sigma\end{aligned} \tag{28}$$

for all $t \ge T_1,\ i=1,2,3$. Q.E.D.

2) Convergence of the ADRC

Let $\left[r_1, r_2, r_3\right]^T = \left[r,\ \dot{r},\ \ddot{r}\right]^T$ and $e_i(t) = r_i(t) - X_i(t)$, $i=1,2$.

Theorem 2: Assuming that h is bounded, there exist a constant $\rho > 0$ and a finite time $T_3 > 0$ such that $\left|e_i(t)\right| \le \rho,\ i=1,2,\forall t \ge T_3 > 0, \omega_o > 0$ and $\omega_c > 0$. Furthermore, $\rho = \mathrm{O}\left(\dfrac{1}{\omega_o^k}\right)$ and $\rho = \mathrm{O}\left(\dfrac{1}{\omega_c^q}\right)$ for some positive integers k and q.

Proof: From (12) and (14), one has

$$\begin{aligned}u_d &= \frac{k_1(r-\hat{x}_1)+k_2(\dot{r}-\hat{x}_2)-\hat{x}_3+\ddot{r}}{b}\\ &= \frac{k_1\left[r_1-(x_1-\tilde{x}_1)\right]+k_2\left[r_2-(x_2-\tilde{x}_2)\right]-(x_3-\tilde{x}_3)+r_3}{b}\\ &= \frac{k_1(e_1+\tilde{x}_1)+k_2(e_2+\tilde{x}_2)-(x_3-\tilde{x}_3)+r_3}{b}.\end{aligned} \tag{29}$$

It follows that

$$\begin{aligned}\dot{e}_1 &= \dot{r}_1-\dot{x}_1 = r_2-x_2 = e_2\\ \dot{e}_2 &= \dot{r}_2-\dot{x}_2 = r_3-(x_3+bu_d)\\ &= r_3-x_3-\left[k_1(e_1+\tilde{x}_1)+k_2(e_2+\tilde{x}_2)-(x_3-\tilde{x}_3)+r_3\right]\\ &= -k_1(e_1+\tilde{x}_1)-k_2(e_2+\tilde{x}_2)-\tilde{x}_3.\end{aligned} \tag{30}$$

Let $e(t) = \left[e_1(t), e_2(t)\right]^T$, $\tilde{X}(t) = \left[\tilde{x}_1(t), \tilde{x}_2(t), \tilde{x}_3(t)\right]^T$, then

$$\dot{e}(t) = A_e e(t) + A_{\tilde{X}}\tilde{X}(t) \tag{31}$$

where $A_e = \begin{bmatrix}0 & 1\\ -k_1 & -k_2\end{bmatrix}$ and $A_{\tilde{X}} = \begin{bmatrix}0 & 0 & 0\\ -k_1 & -k_2 & -1\end{bmatrix}$.

Solving (32), we have

$$e(t) = e^{A_e t}e(0) + \int_0^t e^{A_e(t-\tau)}A_{\tilde{X}}\tilde{X}(\tau)\,d\tau. \tag{32}$$

According to (32) and Theorem 1, one has

$$\begin{aligned}&\left[A_{\tilde{X}}\tilde{X}(\tau)\right]_{i=1} = 0\\ &\left|\left[A_{\tilde{X}}\tilde{X}(\tau)\right]_2\right| = \left|-k_1\tilde{x}_1(\tau)-k_2\tilde{x}_2(\tau)-\tilde{x}_3(\tau)\right|\\ &\qquad \le k_{sum}\sigma = \gamma \text{ for all } t \ge T_1\end{aligned} \tag{33}$$

where $k_{sum} = 1+k_1+k_2$. Let $\varphi(t) = \int_0^t e^{A_e(t-\tau)}A_{\tilde{X}}\tilde{X}(\tau)\,d\tau$. Define $\Psi = \left[0\ \gamma\right]^T$. It follows that

$$\begin{aligned}\left|\varphi_i(t)\right| &= \int_0^t\left[e^{A_e(t-\tau)}A_{\tilde{X}}\tilde{X}(\tau)\right]_i d\tau\\ &\le \int_0^t\left[e^{A_e(t-\tau)}\Psi\right]_i d\tau\\ &\le \left|\left(A_e^{-1}\Psi\right)_i\right| + \left|\left(A_e^{-1}e^{A_e t}\Psi\right)_i\right|.\end{aligned} \tag{34}$$

Since $A_e^{-1} = \begin{bmatrix}-\dfrac{k_2}{k_1} & -\dfrac{1}{k_1}\\ 1 & 0\end{bmatrix} = \begin{bmatrix}-\dfrac{2}{\omega_c} & -\dfrac{1}{\omega_c^2}\\ 1 & 0\end{bmatrix}$, we have

$$\begin{aligned}\left|\left(A_e^{-1}\Psi\right)_1\right| &= \frac{\gamma}{\omega_c^2}\\ \left|\left(A_e^{-1}\Psi\right)_2\right| &= 0.\end{aligned} \tag{35}$$

Since A_e is Hurwitz, there exists a finite time $T_2 > 0$ such that

$$\left|\left[e^{A_e t}\right]_{ij}\right| \le \frac{1}{\omega_c^3} \tag{36}$$

for all $t \ge T_2,\ i,j=1,2$. Note that T_2 depends on A_e. Let $e^{A_e t} = \begin{bmatrix}o_{11} & o_{12}\\ o_{21} & o_{22}\end{bmatrix}$ and $e_{sum}(0) = \left|e_1(0)\right|+\left|e_2(0)\right|$. It follows that

$$\begin{aligned}\left|\left[e^{A_e t}e(0)\right]_i\right| &= \left|o_{i1}e_1(0)+o_{i2}e_2(0)\right|\\ &\le \frac{e_{sum}(0)}{\omega_c^3}\end{aligned} \tag{37}$$

for all $t \ge T_2,\ i=1,2$. Let $T_3 = \max\left\{T_1, T_2\right\}$. We have

$$\left|\left(e^{A_e t}\Psi\right)_i\right| \le \frac{\gamma}{\omega_c^3} \tag{38}$$

for all $t \ge T_3,\ i=1,2$, and

$$\left|\left(A_e^{-1}e^{A_e t}\Psi\right)_i\right| \le \begin{cases}\left|\dfrac{1+2\omega_c}{\omega_c^2}\dfrac{\gamma}{\omega_c^3}\right|_{i=1}\\ \left|\dfrac{\gamma}{\omega_c^3}\right|_{i=2}\end{cases} \tag{39}$$

for all $t \geq T_3$. From (34), (35), and (39), we obtain

$$\begin{aligned} |\varphi_i(t)| &\leq \left|\left(A_e^{-1}\Psi\right)_i\right| + \left|\left(A_e^{-1}e^{A_e t}\Psi\right)_i\right| \\ &\leq \begin{cases} \left|\dfrac{\gamma}{\omega_c^2} + \dfrac{1+2\omega_c}{\omega_c^2}\dfrac{\gamma}{\omega_c^3}\right|_{i=1} \\ \left|\dfrac{\gamma}{\omega_c^3}\right|_{i=2} \end{cases} \end{aligned} \tag{40}$$

for all $t \geq T_3$. From (32), one has

$$|e_i(t)| \leq \left|\left[e^{A_e t}e(0)\right]_i\right| + |\varphi_i(t)|. \tag{41}$$

According to (34), (35), and (37), we have

$$\begin{aligned} |e_i(t)| &\leq \begin{cases} \left|\dfrac{e_{sum}(0)}{\omega_c^3} + \dfrac{\gamma}{\omega_c^2} + \dfrac{\gamma(1+2\omega_c)}{\omega_c^5}\right|_{i=1} \\ \left|\dfrac{e_{sum}(0)+\gamma}{\omega_c^3}\right|_{i=2} \end{cases} \\ &= \begin{cases} \left|\dfrac{e_{sum}(0)}{\omega_c^3} + \dfrac{\left(1+2\omega_c+\omega_c^2\right)\sigma}{\omega_c^2} + \dfrac{\left(1+2\omega_c+\omega_c^2\right)(1+2\omega_c)\sigma}{\omega_c^5}\right|_{i=1} \\ \left|\dfrac{e_{sum}(0)+\left(1+2\omega_c+\omega_c^2\right)\sigma}{\omega_c^3}\right|_{i=2} \end{cases} \\ &\leq \rho \end{aligned} \tag{42}$$

for $t \geq T_3$, $i = 1, 2$, where $\rho = \max\left\{\dfrac{e_{sum}(0)}{\omega_c^3} + \dfrac{\left(1+2\omega_c+\omega_c^2\right)\sigma}{\omega_c^2} + \dfrac{\left(1+2\omega_c+\omega_c^2\right)(1+2\omega_c)\sigma}{\omega_c^5}, \dfrac{e_{sum}(0)+\left(1+2\omega_c+\omega_c^2\right)\sigma}{\omega_c^3}\right\}$. Q.E.D.

IV. SIMULATION RESULTS

We simulate the oscillation controller on the model of a piezoelectrically driven vibrational beam gyroscope [6]. The vibrational beam gyroscope consists of a 20mm-long steal beam and four piezoelectric strips which are attached to each side of the cross-section of the beam. Two of the strips are functioning as actuators, and the other two are acting as sensors. The beam is driven to resonance through one of the piezoelectric actuators. The deformation (or displacement) of the beam is transformed to voltage output through the other piezoelectric actuator. The voltage output of the actuator is proportional to its displacement. As the output is 100mv, the corresponding displacement of the beam gyroscope is approximately 1 micrometer. The natural frequency and damping coefficient of the gyroscope are ω_n=63881.1*rad/s* and ς=*0.0005* $N \cdot s/m$. The desired frequency of drive axis is ω=65973.4 *rad/s (f*=10.17*KHz)*, which is approximately equal to its natural frequency. Normally the displacement output amplitude of drive axis is $A=10^{-6}$ *m*. So we choose 100mv as the desired amplitude of the reference signal. We use *A=0.1* in simulation units to represent this. Then the reference signal *r = 0.1sin (*65973.4*t*). The PSD of mechanical-thermal noise is 4.22×10^{-26} N^2sec according to [8]. We assume the magnitude of Quadrature error term is 0.1% of natural frequency according to [9]. We suppose the rotation rate is constant and $\Omega = 0.1 rad/s$. The coefficient *b=K/m*=271780942.56. For the ADRC and ESO, we choose a controller gain ω_c as 5×10^4 and an observer gain ω_o as 25×10^4. Fig. 2 (a) shows the real output x of drive axis and the reference signal r in the first 1ms. Fig. 2 (b) shows the output x and r in one period which is around 0.1ms as we desired. We can see that after initial deviation, the output x can track the reference signal r very well. Fig. 3 shows the tracking error between the reference signal *r* and the real output of drive axis *x* in different time ranges. The stabilized peak error is around 0.7% of the desired amplitude of the output x. Our simulation results demonstrate the robustness of the oscillation controller against parameter variations (within 40%) and mechanical-thermal noise.

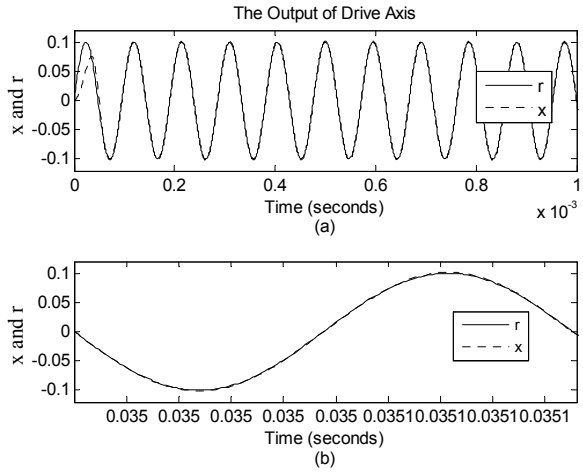

Fig. 2: The output of drive axis and the reference signal

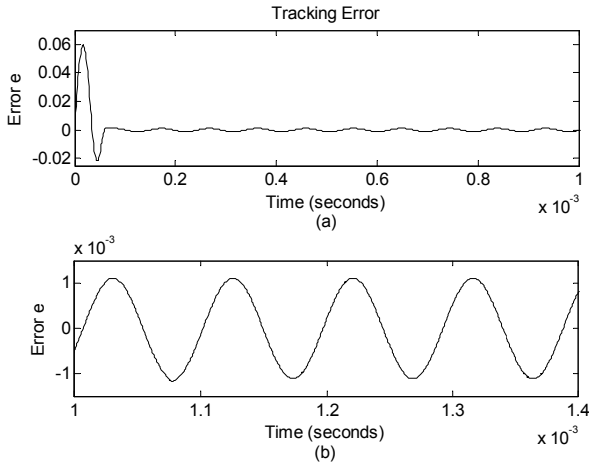

Fig. 3: The tracking error e

V. ANALOG IMPLEMENTATION AND EXPERIMENTAL RESULTS

We conduct the analog implementation of the ADRC onto the drive axis of the vibrational gyroscope because of fast response and low cost of the analog circuit. The setup diagram of the Analog Implementation of the ADRC Using Discrete Components (AIUDC) is shown in Fig.4. In Fig.4, a saturator is used to limit the amplitude of the control signal that prevents the fragile vibrational gyroscope from being broken by possibly large magnitude of the input. We choose 100mv as the desired amplitude of the reference signal. The other parameters of the beam gyroscope are subject to the variations of ±10% in the original values in practice.

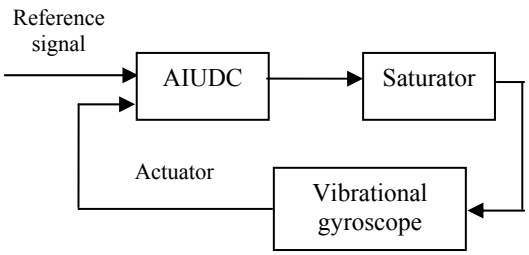

Fig. 4: Setup diagram of analog implementation of ADRC

The reference signal and the real output of the drive axis are given in Fig. 5. The tracking error between the real output and the reference signal is shown in Fig.6. The peak error is about *10%* of the original amplitude, which is bigger than the one in simulation. We believe this is mainly caused by the electronic noise coming from the circuit. However, the analog implementation of the ADRC produces a very fast response as shown in Fig. 7 where the output of the drive axis reaches the desired output within *0.14ms* only. In [6], the same beam gyroscope is used for testing an adaptive controller which is also implemented by an analog circuit. It takes a much longer time (almost *3 seconds*) for the adaptive control system in [6] to reach the steady-state response. In addition, with the application of the ADRC, the vibrational beam gyroscope achieved resonance for a bigger range of the input frequency (*150Hz*) than the range given in [6] (*100Hz*).

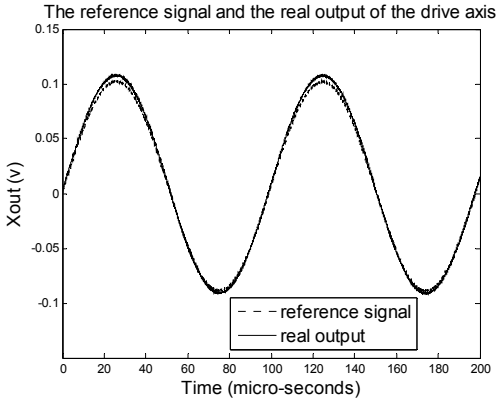

Fig.5: The output of the drive axis and reference signal

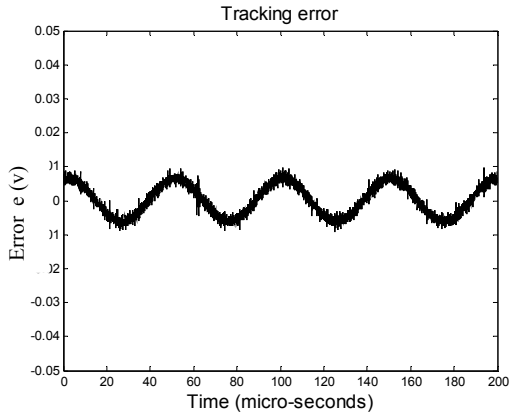

Fig. 6: The tracking error between the reference signal and the real output of the drive axis

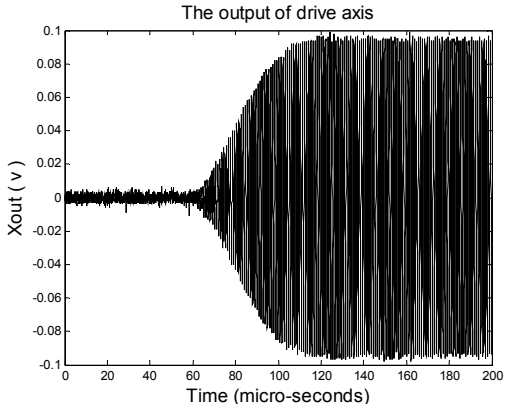

Fig.7: The output of the drive axis

VI. CONCLUDING REMARKS

We explored a new application of the ADRC for controlling the driving mode of vibrational gyroscopes. The stability analysis shows that both the estimation error and the tracking error of the drive axis output are bounded and the upper bounds of the errors monotonously decrease with the increase of observer and controller bandwidths. The simulation and analog results validated the oscillation controller with the chosen controller and observer gains. In our future research, we plan to implement the ADRC on the sense axis of the vibrational gyroscope. We will also explore the possibility of using the ADRC to other MEMS sensors.

REFERENCES

[1] N. Barbour, G. Schemidt, "Inertial sensor technology trends," *IEEE Sensor Journal*, Vol.1, No.4, pp. 332-339, Dec. 2001.

[2] Y. Yazdi, F. Ayazi, and K. Najafi, "Micromachined inertial sensors," in *Proceedings of IEEE*, Vol. 86, No.8, pp.1640-1659, August 1998.

[3] S. Park and R. Horowitz, "Adaptive control for the conventional mode of operation of MEMS gyroscopes," *Journal of Micro-electromechanical Systems*, Vol.12, No.1, pp. 101-108, Feb. 2003.

[4] C. Acar, S. Eler, and A. Shel, "Concept, implementaion, and control of Wide Bandwidth MEMS Gyroscopes," in *Proceedings of American Control Conference*, Arlington, VA, pp.1229-1234, June 2001.

[5] R. T. M'Closkey, A. Vakakis, "Analysis of a micromsensor automatic gain control loop," in *Proceedings of American Control Conference*, San Diego, CA, pp. 3307-3311, June 1999.

[6] R. P. Leland, "Adaptive tuning for vibrational gyroscopes," in *Proceedings of 40th IEEE Conference on Decision and Control*, Orlando, FL, pp. 3447-3452, Dec. 2001.

[7] R. P. Leland, Y. Lipkin, and A. Highsmith, "Adaptive oscillator control for a vibrational gyroscope," in *Proceedings of American Control Conference*, Denver, CO, pp. 3347-3352, June 2003.

[8] S. Park, "Adaptive control strategies for MEMS gyroscopes," Ph.D. dissertation, University of California, Berkeley, 2000.

[9] L. Dong and R. P. Leland, "The adaptive control System of a MEMS gyroscope with time-varying rotation rate," in *Proceedings of American Control Conference*, Portland, OR, pp. 3592-3597, June 2005.

[10] Z. Gao, "Active disturbance rejection control: a paradigm shift in feedback control system design," in *proceedings of American Control Conference*, Minneapolis, MN, June 2006.

[11] Z. Gao, "Scaling and bandwidth-parameterization based controller tuning," in *Proceedings of American Control Conference*, Denver, CO, Vol. 6, pp.4989-4996, June 2003.

[12] Z. Gao, Y. Huang, J. Han, "A novel motion control design approach based on active disturbance rejection," in *IEEE Conference on Decision and Control*, Orlando, FL, Vol.5, pp. 4578-4585, Dec. 2001.